Data report: component and grain size analysis of visible tephra layers, Cores 1H through 6H, Holes U1396A and U1396B, southwest Montserrat[1]

Adam J. Stinton[2, 3]

Chapter contents

[1] Stinton, A.J., 2016. Data report: component and grain size analysis of visible tephra layers, Cores 1H through 6H, Holes U1396A and U1396B, southwest Montserrat. *In* Le Friant, A., Ishizuka, O., Stroncik, N.A., and the Expedition 340 Scientists, *Proceedings of the Integrated Ocean Drilling Program,* 340: Tokyo (Integrated Ocean Drilling Program Management International, Inc.). doi:10.2204/iodp.proc.340.205.2016
[2] Montserrat Volcano Observatory, Flemmings, Montserrat, West Indies. adam@mvo.ms
[3] Also at Seismic Research Centre, University of the West Indies, St. Augustine, Trinidad and Tobago.

Abstract

Integrated Ocean Drilling Program Expedition 340 recovered up to 138 m of continuous core from Site U1396, 55 km southwest of Montserrat. The recovered section contains >180 visible tephra layers dating to ~4.5 Ma. Of these, the uppermost 70 tephra layers date to 2.5 Ma, covering the period of known subaerial volcanism on Montserrat. Each tephra sample underwent component analysis through point counting and grain size analysis with a Malvern Mastersizer 2000 particle size analyzer. Component analysis shows that the tephras are dominated by grains consisting of glass shards and crystals. A small number of samples from within Core 340-U1396A-6H contained scoria. Grain size analysis showed that most tephras consist of fine to medium sand and are poorly to moderately sorted.

Introduction

Integrated Ocean Drilling Program Expedition 340 investigated volcaniclastic sediments and landslide deposits in the Lesser Antilles arc with the primary objective of furthering understanding of the evolution and eruptive history of the arc, as well as gaining insight into the emplacement of large landslides and debris avalanches in the submarine environment along the Lesser Antilles arc.

During Expedition 340, four sites adjacent to the island of Montserrat, in the northern part of the Lesser Antilles arc (Fig. F1), were drilled. One of these sites, U1396, was drilled in order to recover cores for investigation of the long-term volcanic history of Montserrat. Site U1396 is located 55 km southwest of Montserrat on a topographic high. A detailed overview of Site U1396 geography, objectives, and preliminary results is provided by Le Friant et al. (2015) and is in the "Expedition 340 summary" chapter (Expedition 340 Scientists, 2013). Drilling at Site U1396 recovered cores from three holes. Holes U1396A and U1396C are continuous to ~138 meters below seafloor (mbsf), whereas core recovered from Hole U1396B was used to supplement a section of core in Hole U1396A that was disturbed during recovery. All samples analyzed in this data report are from cores recovered from Holes U1396A and U1396B.

Over the last 20 y, Montserrat has been the focus of considerable work on the processes, deposits, and effects of volcanism in both

doi:10.2204/iodp.proc.340.205.2016

subaerial and submarine environments (e.g., Aspinall et al., 1998; Young et al., 1998; Druit and Kokelaar, 2002; Wadge et al., 2014). However, the majority of the research has been on the Soufriere Hills Volcano, which has been erupting since July 1995. Consequently, only limited data on the history of the older volcanic centers on Montserrat exists. At present, studies of Montserrat have identified three main centers of volcanism; starting with the oldest they are Silver Hills (~2600 to ~1200 ka), Centre Hills (950–550 ka), and the South Soufriere Hills-Soufriere Hills (~282 ka to present) (Roobol and Smith, 1998; Harford et al., 2002; Smith et al., 2007; Le Friant et al., 2008).

During onboard and postcruise core description and logging, 187 visible tephra layers were identified in Hole U1396A (including 9 in Core 340-U1396A-2H). A further 11 visible tephra layers were identified in core recovered from Hole U1396B, giving a total of 190 visible tephra layers in the combined Holes U1396A and U1396B stratigraphy. According to preliminary paleomagnetic ages determined on board the R/V *JOIDES Resolution* during Expedition 340, the oldest tephra dates to 4.45 Ma (the early Pliocene), ~2 m.y. older than the oldest known age for subaerial volcanism on Montserrat. For the purposes of this data report, the focus has been on analysis of samples from visible tephra layers within the uppermost six cores recovered (i.e., the uppermost 53 mbsf). The oldest tephra has a paleomagnetic age of ~2.5 Ma and therefore corresponds to the oldest known age for subaerial volcanism on Montserrat.

Methods

Each of the 70 visible tephra layers identified in Cores 340-U1396A-1H through 6H (excluding Core 2H) and Core 340-U1396B-2H have been analyzed for their components and particle grain size using the methods outlined below.

Components

Samples measuring ~0.5 cm^3 were taken from each visible tephra layer and dried at 60°C. The samples were then washed with deionized water over a 63 µm sieve to remove the fine-grained hemipelagic component. Following this, 2.5 mL of acetic acid (20%) was added to the sample and left for up to 4 h to dissolve the biogenic carbonate. The samples were then again washed and dried in an oven at 55°C. Component analysis was performed by placing aliquots of individual samples on a gridded microscope slide and point-counting an average of 400 grains per sample. The grains were classified according to one of six categories, following the previous studies of Cassidy et al. (2013, 2014). The six categories are as follows:

1. Nonvesicular dense juvenile lava clasts,
2. Vesicular juvenile lava clasts,
3. Altered lava clasts,
4. Crystals (including glass shards),
5. Scoria, and
6. Biogenic material.

Descriptions and examples of these categories can be found in Cassidy et al. (2013). Glass shards and crystals have been combined into one category because of the difficulty of differentiating between the two components under a normal, nonpolarized microscope (Enache and Cumming, 2006; Cassidy et al., 2013, 2014) such as the Meiji EMZ-5 binocular microscope used in this study. Some studies have previously excluded the biogenic components of samples from the point counts; they are included here for completeness, as it may be possible to infer something about transport or environment effects during deposition of the tephra layer if large proportions of biogenic material are present.

Grain size

Small subsamples of each tephra layer were first washed over a 1000 µm (1 mm) sieve and then disaggregated by placing on a shaking table overnight in 25 mL of reverse-osmosis water that contained 0.05% sodium hexametaphosphate dispersant. The dispersed sediment solutions were analyzed with a Malvern Mastersizer 2000 particle size analyzer, which is capable of measuring particles with sizes between 0.02 and 2000 µm. The grain size data collected by the Malvern Mastersizer is a volume percent of the sample. Grain size data were then analyzed with the GRADISTAT software (Blott and Pye, 2001) to calculate sorting coefficients according to the Folk and Ward (1957) method.

Results

Components

Results of the component analysis for the 70 visible tephra layers identified in Cores 1H through 6H in Holes U1396A and U1396B are presented in Table **T1**. A summary of the component analysis is presented in Table **T2,** which clearly shows that of the six component categories used to classify grains, samples are dominated by crystals and glass shards, with vesicular lava clasts and nonvesicular dense clasts in order of decreasing abundance. Glass shards and crystals are the most abundant component and are present in all 70 tephra layers, varying between 18% and 96% of grains per sample. Within this wide

range, 58 of the 70 tephra layers contain >40% glass shards and crystals. There appears to be no pattern to the depth of tephra layers containing the highest abundances of glass and crystals within Holes U1396A and U1396B. The second most abundant component is juvenile vesicular clasts, which varies between 1.3% and 76.6%. Of the 67 tephra layers that contain juvenile vesicular clasts, 19 contain >30% juvenile vesicular clasts. As with the glass shards and crystals component, there appears to be no pattern to the depth of tephra layers containing the highest abundances of juvenile vesicular clasts within Holes U1396A and U1396B. Juvenile dense clasts are the third most abundant component, varying from 0.2 to 47.9%, with 10 samples containing >20% juvenile dense clasts. In terms of the vertical distribution through the cores, 8 of the 10 tephra layers with >20% juvenile dense clasts were found in Core 340-U1396A-6H. Of the remaining components, scoria clasts (0.5%–45.1%) were found in only 12 tephra layers. All scoria-bearing tephra layers were found within Core 6H. Several examples of samples containing high abundances of two or more components were found. For example, Sample 340-U1396A-6H-5, 144–145 cm, contains >30% vesicular juvenile components and >56% glass shards and crystals, whereas Sample 6H-7, 5–6 cm, contains 50% glass shards and crystals and 45% scoria.

Grain size

The results of the grain size analysis are presented in Figure F2, whereas summary statistics derived using the GRADISTAT software are provided in Table T3. Grain size distributions presented graphically in Figure F2 show wide variation in the nature of the distributions, from predominantly fine grained to strongly coarse grained tephras, as well as unimodal, biomodal, and distributions with multiple populations. The summary statistics presented in Table T3, derived from GRADISTAT software (Blott and Pye, 2001), show that the majority of tephra layers (59 out of 69; 86%) display either unimodal or bimodal distributions, with the rest being either trimodal (eight tephra layers) or polymodal (two tephra layers). Core 340-U1396A-6H contains most (14 out of 30; 47%) of the tephra layers with a unimodal grain size distribution.

The sorting and mean grain size of the tephra layers varies considerably, ranging from very well sorted very fine sand to poorly sorted coarse sand. However, the majority of tephra layers contain fine or medium sand (48 out of 69; 70%) and are poorly to moderately sorted (49 out of 69; 71%). The shape of the grain size distributions, as shown graphically in Figure F2, also varies considerably, with distributions covering the entire range of values skewed strongly to the fine grain sizes through those skewed strongly to coarse grain sizes. However, approximately one-third (26 out of 69) of the tephra layers have a symmetrical distribution around the mean grain size. Values for kurtosis, or degree of peakedness, of the grain size distributions show that most tephra layers (53 out of 69; 78%) display a platykurtic- or mesokurtic-shaped curve, indicating that the tails of the curves are better sorted than the center region. Platykurtic- or mesokurtic-shaped curves have a flat shape and would be associated with either symmetrical or slightly skewed grain size distributions.

Acknowledgments

All members of the onboard core description team are gratefully acknowledged for their tremendous effort to log and described the core recovered at Site U1396. Samples were taken during the postcruise sampling party at the Integrated Ocean Drilling Program (IODP) Gulf Coast Core Repository at Texas A&M University. Sample preparation was conducted at the National Oceanography Centre, University of Southampton, United Kingdom, during a stint as a visiting researcher funded by a personal travel grant from the University of West Indies, St. Augustine, Trinidad and Tobago. Assistance at NOC-UoS was provided by Professor M. Palmer and Dr. M. Cassidy.

References

Aspinall, W.P., Lynch, L.L., Robertson, R.E.A., Rowley, K., Sparks, R.S.J., Voight, B., and Young, S.R., 1998. The Soufriere Hills eruption, Montserrat, British West Indies: introduction to Special Section, Part 1. *Geophysical Research Letters,* 25(18):3387. **http://dx.doi.org/10.1029/98gl02438**

Blott, S.J., and Pye, K., 2001. GRADISTAT: a grain size distribution and statistics package for the analysis of unconsolidated sediments. *Earth Surface Processes and Landforms,* 26(11):1237–1248. **http://dx.doi.org/10.1002/esp.261**

Cassidy, M., Trofimovs, J., Palmer, M.R., Talling, P.J., Watt, S.F.L., Moreton, S.G., and Taylor, R.N., 2013. Timing and emplacement dynamics of newly recognised mass flow deposits at ~8–12 ka offshore Soufrière Hills volcano, Montserrat: how submarine stratigraphy can complement subaerial eruption histories. *Journal of Volcanology and Geothermal Research,* 253:1–14. **http://dx.doi.org/10.1016/j.jvolgeores.2012.12.002**

Cassidy, M., Watt, S.F.L., Palmer, M.R., Trofimovs, J., Symons, W., Maclachlan, S.E., and Stinton, A.J., 2014. Construction of volcanic records from marine sediment cores: a review and case study (Montserrat, West Indies). *Earth-Science Reviews,* 138:137–155. **http://dx.doi.org/10.1016/j.earscirev.2014.08.008**

Druitt, T.H., and Kokelaar, B.P., 2002. The eruption of Soufrière Hills Volcano, Montserrat, from 1995 to 1999. *Memoir—Geological Society of London,* 21:45–69. **http://dx.doi.org/10.1144/GSL.MEM.2002.021.01.32**

Enache, M.D., and Cumming, B.F., 2006. The morphological and optical properties of volcanic glass: a tool to assess density-induced vertical migration of tephra in sediment cores. *Journal of Paleolimnology,* 35(3):661–667. **http://dx.doi.org/10.1007/s10933-005-3604-9**

Expedition 340 Scientists, 2013. Expedition 340 summary. *In* Le Friant, A., Ishizuka, O., Stroncik, N.A., and the Expedition 340 Scientists, *Proceedings of the Integrated Ocean Drilling Program,* 340: Tokyo (Integrated Ocean Drilling Program Management International, Inc.). **http://dx.doi.org/10.2204/iodp.proc.340.101.2013**

Folk, R.L., and Ward, W.C., 1957. Brazos River bar [Texas]: a study in the significance of grain size parameters. *Journal of Sedimentary Research,* 27(1):3–26. **http://dx.doi.org/10.1306/74D70646-2B21-11D7-8648000102C1865D**

Harford, C.L., Pringle, M.S., Sparks, R.S.J., and Young, S.R., 2002. The volcanic evolution of Montserrat using $^{40}Ar/^{39}Ar$ geochronology. *Memoir—Geological Society of London,* 21:93–113. **http://dx.doi.org/10.1144/GSL.MEM.2002.021.01.05**

Le Friant, A., Ishizuka, O., Boudon, G., Palmer, M.R., Talling, P.J., Villemant, B., Adachi, T., Aljahdali, M., Breitkreuz, C., Brunet, M., Caron, B., Coussens, M., Deplus, C., Endo, D., Feuillet, N., Fraas, A.J., Fujinawa, A., Hart, M.B., Hatfield, R.B., Hornbach, M., Jutzeler, M., Kataoka, K.S., Komorowski, J.-C., Lebas, E., Lafuerza, S., Maeno, F., Manga, M., Martínez-Colon, M., McCanta, M., Morgan, S., Saito, T., Slagle, A., Sparks, S., Stinton, A., Stroncik, N., Subramanyam, K.S.V., Tamura, Y., Trofimovs, J., Voight, B., Wall-Palmer, D., Wang, F., and Watt, S.F.L., 2015. Submarine record of volcanic island construction and collapse in the Lesser Antilles arc: first scientific drilling of submarine volcanic island landslides by IODP Expedition 340. *Geochemistry, Geophysics, Geosystems,* 16(2):420–442. **http://dx.doi.org/10.1002/2014GC005652**

Le Friant, A., Lock, E.J., Hart, M.B., Boudon, G., Sparks, R.S.J., Leng, M.J., Smart, C.W., Komorowski, J.C., Deplus, C., and Fisher, J.K., 2008. Late Pleistocene tephrochronology of marine sediments adjacent to Montserrat, Lesser Antilles volcanic arc. *Journal of the Geological Society (London, U. K.),* 165(1):279–289. **http://dx.doi.org/10.1144/0016-76492007-019**

Roobol, M.J., and Smith, A.L., 1998. Pyroclastic stratigraphy of the Soufrière Hills Volcano, Montserrat—implications for the present eruption. *Geophysical Research Letters*, 25(18):3393–3396. **http://dx.doi.org/10.1029/98GL00643**

Smith, A.L., Roobol, M.J., Schellekens, J.H., and Mattioli, G.S., 2007. Prehistoric stratigraphy of the Soufrière Hills–South Soufrière Hills volcanic complex, Montserrat, West Indies. *The Journal of Geology*, 115(1):115–127. **http://dx.doi.org/10.1086/509271**

Wadge, G., Voight, B., Sparks, R.S.J., Cole, P.D., Loughlin, S.C., and Robertson, R.E.A., 2014. An overview of the eruption of Soufrière Hills Volcano, Montserrat from 2000 to 2010. *Memoirs—Geological Society of London*, 39:1–40. **http://dx.doi.org/10.1144/M39.1**

Young, S.R., Voight, B., Sparks, R.S.J., Rowley, K., Robertson, R.E.A., Lynch, L.L., and Aspinall, W.P., 1998. The Soufrière Hills eruption, Montserrat, British West Indies: introduction to Special Section, Part 2. *Geophysical Research Letters,* 25(19):3651. **http://dx.doi.org/10.1029/98GL02437**

Initial receipt: 6 May 2015
Acceptance: 12 September 2016
Publication: 4 November 2016
MS 340-205

Figure F1. Location of Site U1396 in relation to the islands of Antigua, Montserrat, and Guadeloupe, in the northeast Lesser Antilles. Basemap data from **http://www.naturalearthdata.com.**

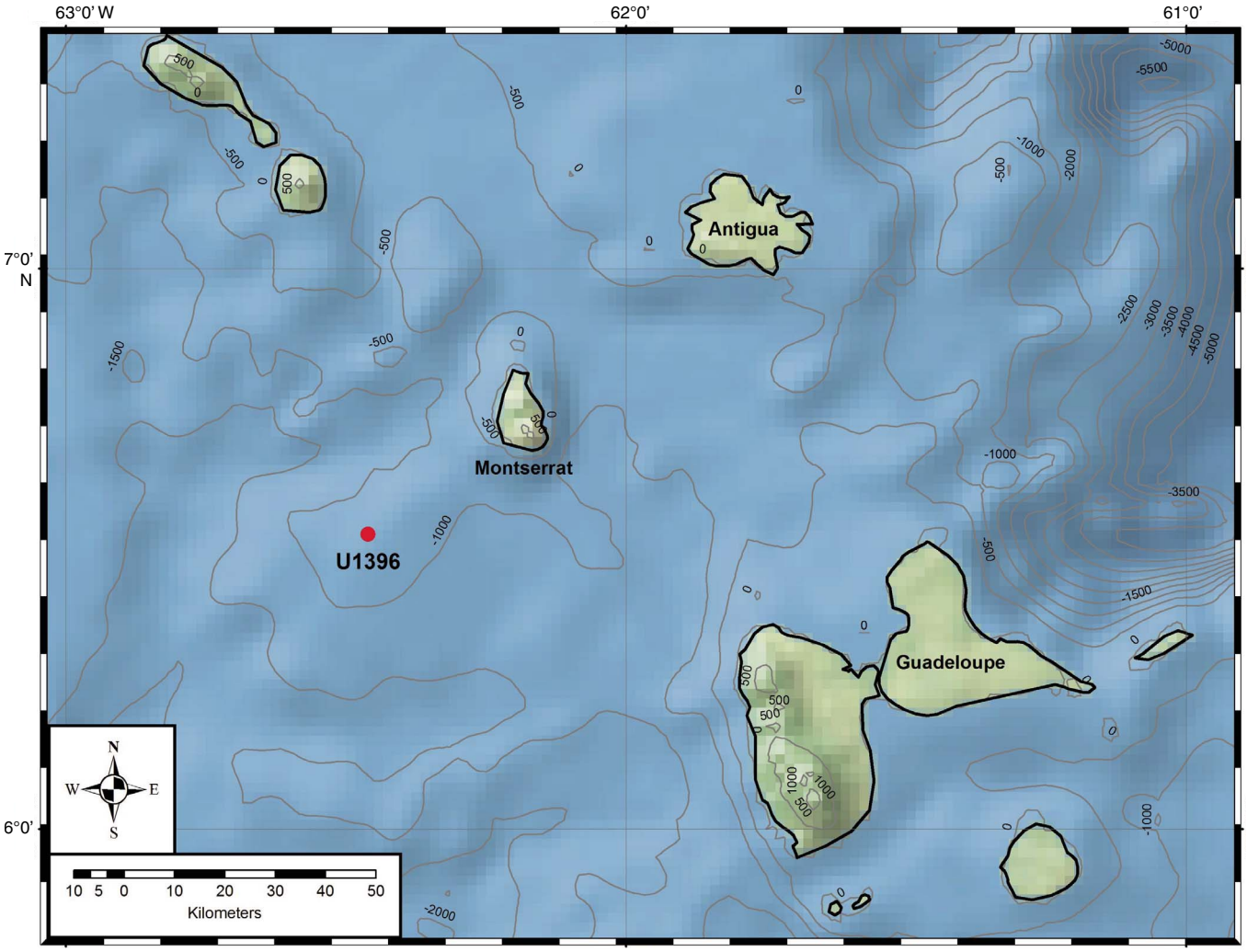

Figure F2. A–C. Grain size distribution plots for each of the visible tephra layers analyzed in Cores 340-U1396A-1H and 3H through 6H and Core 340-U1396B-2H. Data generated by a Malvern Mastersizer 2000 particle size analyzer. (Continued on next page.)

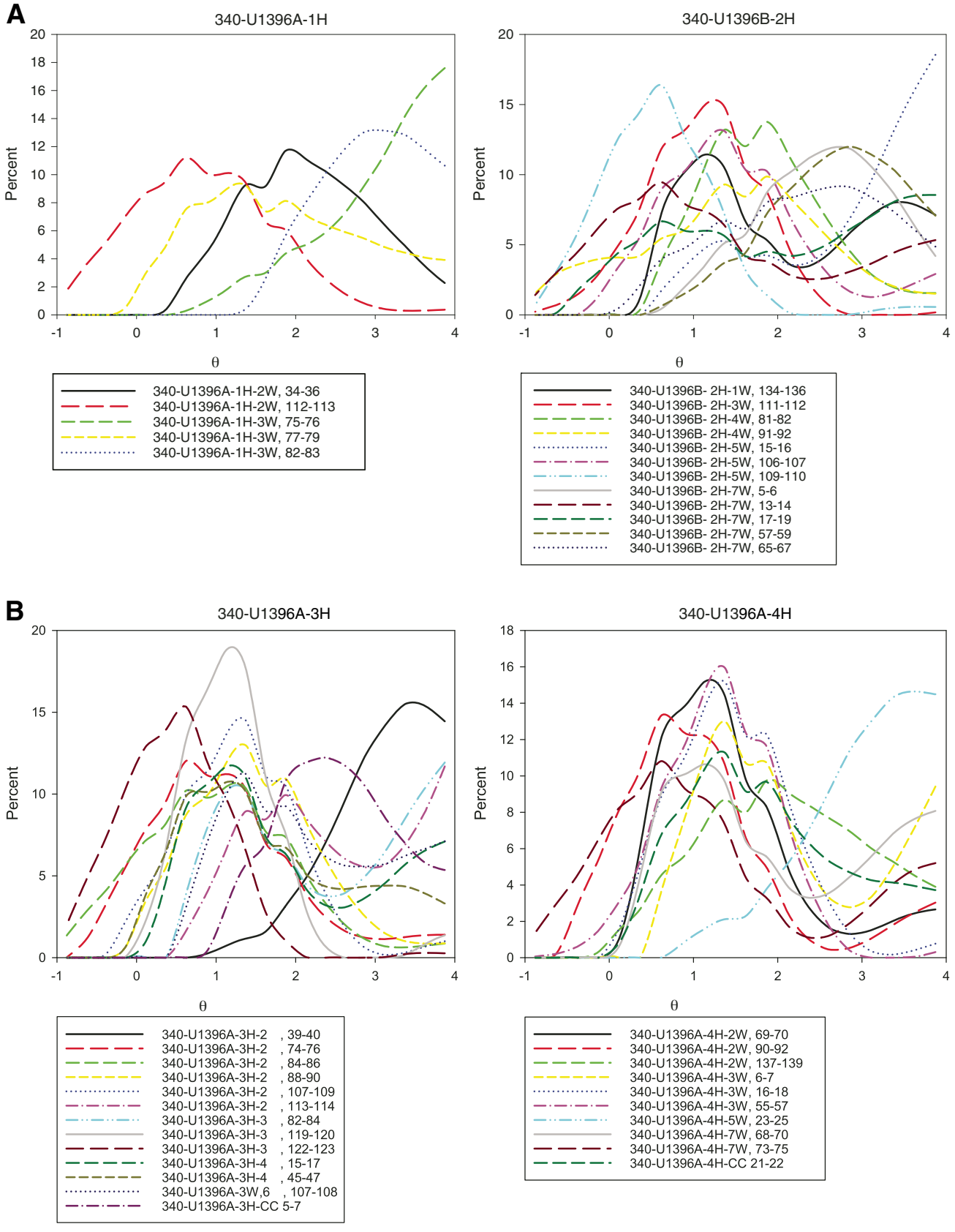

Figure F2 (continued).

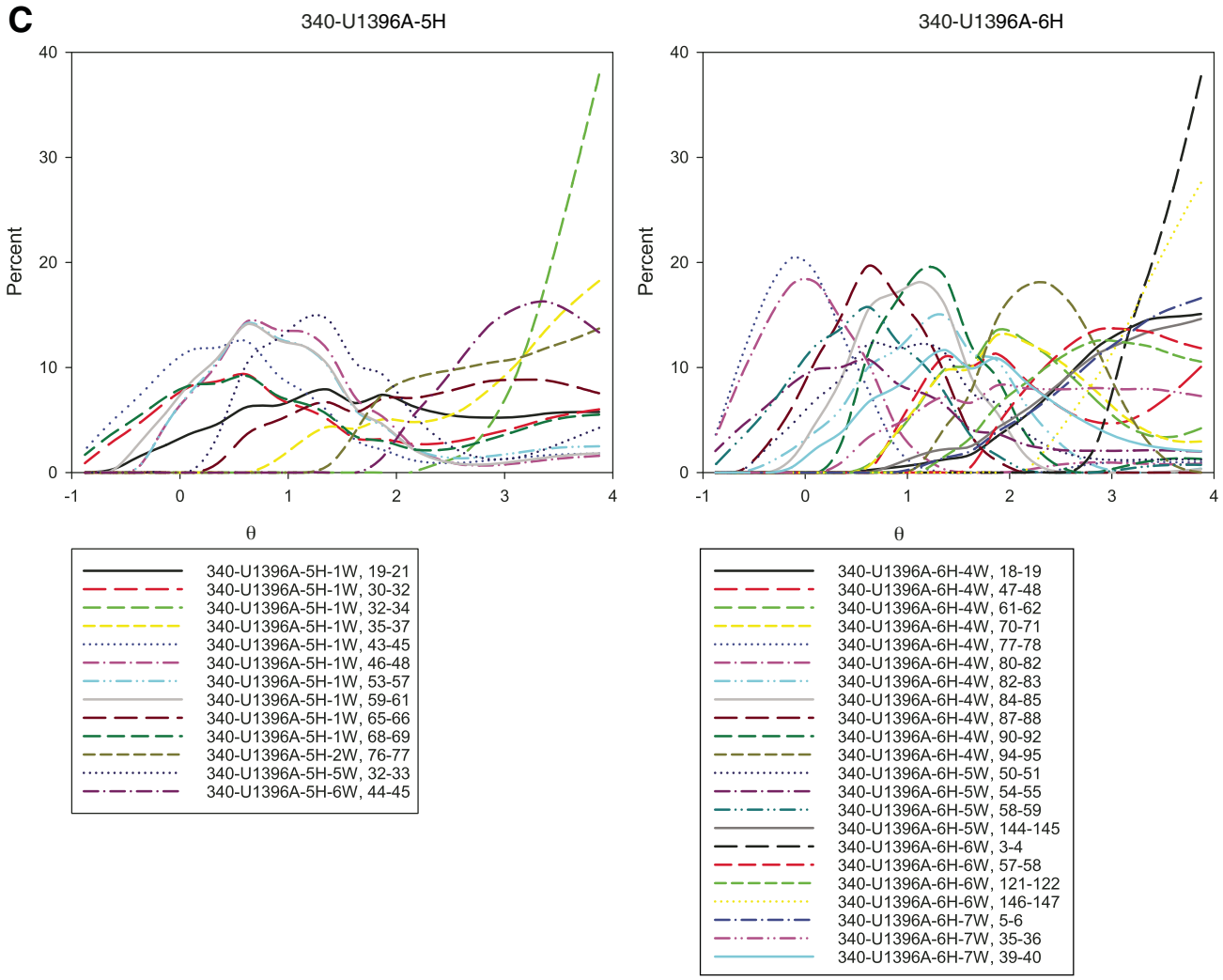

Table T1. Component percentages for visible tephra layers in Cores 1H through 6H, in Holes U1396A and U1396B. (Continued on next page.)

Hole, core, section, interval (cm)	Component (%)					
	Nonvesicular	Vesicular	Altered lava	Crystals and glass shards	Scoria	Biogenic
340-						
U1396A-1H-2, 34–36	8.3	5.4	7.7	78.6	0.0	0.0
U1396A-1H-2, 112–113	8.8	11.2	6.6	73.4	0.0	0.0
U1396A-1H-3, 75–76	2.3	23.6	7.5	65.2	0.0	1.4
U1396A-1H-3, 77–79	0.5	0.0	4.0	95.6	0.0	0.0
U1396A-1H-3, 82–83	4.5	7.0	7.4	79.6	0.0	1.6
U1396B-2H-1, 134–136	16.9	20.4	2.4	48.4	0.0	11.8
U1396B-2H-3, 111–112	9.6	9.9	3.1	77.4	0.0	0.0
U1396B-2H-4, 81–82	1.0	28.3	2.1	68.6	0.0	0.0
U1396B-2H-4, 91–92	13.5	3.5	3.5	63.4	0.0	16.1
U1396B-2H-5, 106–107	34.0	4.5	11.1	49.5	0.0	0.9
U1396B-2H-5, 109–110	21.8	50.5	0.9	26.9	0.0	0.0
U1396B-2H-7, 5–6	4.8	3.6	5.5	84.6	0.0	1.5
U1396B-2H-7, 13–14	2.4	32.7	2.6	62.4	0.0	0.0
U1396B-2H-7, 17–18	0.2	34.7	3.4	60.2	0.0	1.4
U1396B-2H-7, 57–59	9.4	23.3	2.8	63.6	0.0	0.9
U1396B-2H-7, 65–67	1.7	19.7	0.9	75.9	0.0	1.7
U1396A-3H-2, 39–40	0.2	47.1	5.6	46.5	0.0	0.6
U1396A-3H-2, 74–76	3.8	17.0	0.0	52.4	0.0	26.9
U1396A-3H-2, 84–86	0.0	9.2	7.4	83.0	0.5	0.0
U1396A-3H-2, 88–90	8.0	5.2	8.5	78.3	0.0	0.0
U1396A-3H-2, 107–109	3.1	18.9	0.2	77.8	0.0	0.0
U1396A-3H-2, 113–114	7.5	31.1	1.9	59.3	0.0	0.2
U1396A-3H-3, 82–84	2.2	40.6	3.7	43.2	0.0	10.3
U1396A-3H-3, 119–120	2.6	5.0	1.0	91.4	0.0	0.0
U1396A-3H-3, 122–123	8.7	15.2	0.7	75.4	0.0	0.0
U1396A-3H-4, 15–17	1.2	3.8	3.1	60.4	0.0	31.5
U1396A-3H-4, 45–47	1.9	10.1	5.8	62.6	0.0	19.6
U1396A-4H-2, 69–70	3.1	12.3	1.2	83.4	0.0	0.0
U1396A-4H-2, 90–92	0.2	17.9	0.0	81.9	0.0	0.0
U1396A-4H-2, 137–139	18.0	1.3	1.1	64.0	0.0	15.6
U1396A-4H-3, 6–7	0.0	63.5	0.0	24.1	0.0	12.4
U1396A-4H-3, 16–18	0.0	5.6	2.1	92.3	0.0	0.0
U1396A-4H-3, 55–57	1.7	9.7	12.7	71.8	0.0	4.1
U1396A-4H-5, 23–25	4.2	26.6	8.4	60.9	0.0	0.0
U1396A-4H-7, 68–70	0.8	8.4	0.8	66.9	0.0	22.9
U1396A-4H-7, 73–75	0.2	52.0	15.5	32.3	0.0	0.0
U1396A-5H-1, 19–21	0.4	26.6	1.0	56.5	0.0	15.5
U1396A-5H-1, 30–32	2.9	37.2	1.4	56.5	0.9	1.1
U1396A-5H-1, 35–37	1.0	39.7	3.3	51.9	0.0	4.1
U1396A-5H-1, 43–45	2.0	44.1	2.9	50.0	0.0	1.0
U1396A-5H-1, 46–47	2.4	32.6	2.9	61.7	0.0	0.5
U1396A-5H-1, 53–54	3.2	18.4	1.2	77.0	0.0	0.2
U1396A-5H-1, 59–61	2.9	25.3	3.4	67.1	0.0	1.2
U1396A-5H-1, 65–66	2.5	30.0	7.8	58.8	0.0	0.9
U1396A-5H-1, 68–69	9.6	24.7	11.1	54.6	0.0	0.0
U1396A-5H-2, 76–77	0.0	39.2	2.2	55.6	0.0	2.9
U1396A-5H-5, 32–33	4.7	14.4	3.5	75.7	0.0	1.7
U1396A-5H-6, 44–45	0.0	16.0	0.0	84.0	0.0	0.0
U1396A-6H-4, 18–19	6.2	6.5	5.7	39.5	35.5	6.7
U1396A-6H-4, 47–48	2.3	76.6	0.6	18.7	1.9	0.0
U1396A-6H-4, 61–62	19.6	44.0	0.9	35.5	0.0	0.0
U1396A-6H-4, 70–71	32.9	17.2	1.9	48.0	0.0	0.0
U1396A-6H-4, 77–78	19.6	55.9	0.0	24.3	0.0	0.2
U1396A-6H-4, 80–82	22.1	31.0	15.2	31.7	0.0	0.0
U1396A-6H-4, 82–83	25.5	12.0	1.5	41.4	19.0	1.2
U1396A-6H-4, 84–85	35.8	25.5	9.8	28.9	0.0	0.0
U1396A-6H-4, 87–88	14.5	14.0	4.9	37.8	28.7	0.0
U1396A-6H-4, 90–92	12.1	14.6	8.6	28.9	35.8	0.0
U1396A-6H-4, 93–94	47.9	15.7	8.1	27.3	0.5	0.5
U1396A-6H-4, 94–95	10.2	0.0	2.9	45.3	41.6	0.0
U1396A-6H-5, 50–51	19.6	25.4	5.4	48.7	0.0	0.9
U1396A-6H-5, 54–55	27.7	10.2	6.6	55.6	0.0	0.0
U1396A-6H-5, 58–59	31.3	19.4	2.1	46.7	0.5	0.0
U1396A-6H-5, 144–145	9.0	36.0	1.4	52.9	0.7	0.0
U1396A-6H-6, 3–4	20.9	29.7	3.2	45.5	0.0	0.7

Table T1 (continued).

Hole, core, section, interval (cm)	Component (%)					
	Nonvesicular	Vesicular	Altered lava	Crystals and glass shards	Scoria	Biogenic
U1396A-6H-6, 121–122	7.3	10.9	5.3	76.1	0.0	0.4
U1396A-6H-6, 146–147	17.0	29.1	5.8	46.6	0.0	1.4
U1396A-6H-7, 5–6	0.4	0.0	2.6	50.4	45.1	1.4
U1396A-6H-7, 35–36	1.1	30.6	0.7	64.7	0.0	2.9
U1396A-6H-7, 39–40	0.2	23.8	2.2	73.7	0.0	0.0

Table T2. Summary statistics for component analysis of 65 visible tephra layers presented in Table T1.

	Nonvesicular	Vesicular	Altered lava	Crystals and glass shards	Scoria	Biogenic
Number of samples:	5 (>30%)	19 (>30%)	0	58 (>40%)	6 (>10%)	0
Minimum value (%):	0.0	0.0	0.0	18.7	0.0	0.0
Maximum value (%):	47.9	76.6	15.5	95.6	45.1	31.5
Average (%):	8.9	22.2	4.1	58.5	3.0	3.2

Table T3. Summary statistics derived from analysis of grain size data from 69 visible tephra layers using GRADISTAT software (Blott and Pye, 2001). Parameters are determined according to the Folk and Ward (1957) method and reported here as values of φ. (Continued on next page.)

Hole, core, section, interval (cm)	Distribution type	Sediment name	Mean (M_Z)	Sorting (σ_I)	Skewness (Sk_I)	Kurtosis (K_G)
340-						
U1396A-1H-2, 34–36	Unimodal	Moderately sorted medium sand	2.02	0.84	0.06	0.92
U1396A-1H-2, 112–113	Bimodal	Moderately sorted coarse sand	0.71	0.90	0.06	0.95
U1396A-1H-3, 75–76	Unimodal	Moderately sorted very fine sand	2.91	0.79	–0.36	0.93
U1396A-1H-3, 77–79	Bimodal	Poorly sorted medium sand	1.73	1.09	0.13	0.85
U1396A-1H-3, 82–83	Unimodal	Moderately well sorted fine sand	2.82	0.66	–0.07	0.85
U1396B-2H-1, 134–136	Bimodal	Poorly sorted medium sand	1.97	1.12	0.23	0.64
U1396B-2H-3, 111–112	Unimodal	Moderately well sorted medium sand	0.98	0.67	–0.04	0.97
U1396B-2H-4, 81–82	Bimodal	Moderately sorted medium sand	1.72	0.75	0.13	1.01
U1396B-2H-4, 91–92	Bimodal	Poorly sorted medium sand	1.32	1.15	–0.10	1.01
U1396B-2H-5, 106–107	Trimodal	Moderately sorted medium sand	1.33	0.91	0.19	1.23
U1396B-2H-5, 109–110	Unimodal	Moderately well sorted coarse sand	0.43	0.64	0.02	0.98
U1396B-2H-7, 5–6	Unimodal	Moderately sorted fine sand	2.42	0.79	–0.07	0.92
U1396B-2H-7, 13–14	Bimodal	Poorly sorted coarse sand	1.29	1.43	0.32	0.83
U1396B-2H-7, 17–18	Polymodal	Poorly sorted very fine sand	1.94	1.33	–0.08	0.67
U1396B-2H-7, 57–59	Unimodal	Moderately sorted fine sand	2.57	0.79	–0.11	0.92
U1396B-2H-7, 65–67	Trimodal	Poorly sorted fine sand	2.17	1.00	–0.09	0.85
U1396A-3H-2, 39–40	Unimodal	Moderately well sorted very fine sand	2.97	0.64	–0.21	0.92
U1396A-3H-2, 74–76	Bimodal	Moderately sorted coarse sand	0.91	0.93	0.17	1.14
U1396A-3H-2, 84–86	Bimodal	Moderately sorted coarse sand	0.88	0.94	0.02	0.98
U1396A-3H-2, 88–90	Bimodal	Moderately sorted medium sand	1.34	0.80	0.08	1.00
U1396A-3H-2, 107–109	Unimodal	Moderately sorted medium sand	1.15	0.71	0.01	0.97
U1396A-3H-2, 113–114	Trimodal	Poorly sorted medium sand	2.31	1.01	0.12	0.70
U1396A-3H-3, 82–84	Bimodal	Poorly sorted very fine sand	2.21	1.11	0.08	0.61
U1396A-3H-3, 119–120	Unimodal	Moderately well sorted medium sand	1.03	0.53	0.05	1.00
U1396A-3H-3, 122–123	Unimodal	Moderately well sorted coarse sand	0.33	0.65	–0.01	0.94
U1396A-3H-4, 15–17	Bimodal	Poorly sorted medium sand	1.79	1.17	0.37	0.72
U1396A-3H-4, 45–47	Bimodal	Poorly sorted coarse sand	1.56	1.11	0.30	0.85
U1396A-4H-2, 69–70	Bimodal	Moderately sorted medium sand	1.25	0.84	0.31	1.31
U1396A-4H-2, 90–92	Trimodal	Moderately sorted coarse sand	0.88	0.97	0.26	1.46
U1396A-4H-2, 137–139	Bimodal	Poorly sorted medium sand	1.95	1.01	0.05	0.89
U1396A-4H-3, 6–7	Trimodal	Poorly sorted medium sand	2.03	1.07	0.35	0.75
U1396A-4H-3, 16–18	Bimodal	Moderately well sorted medium sand	1.30	0.67	0.05	0.96
U1396A-4H-3, 55–57	Unimodal	Moderately well sorted medium sand	1.17	0.65	–0.03	0.96
U1396A-4H-5, 23–25	Unimodal	Moderately sorted very fine sand	2.91	0.72	–0.25	0.95
U1396A-4H-7, 68–70	Bimodal	Poorly sorted coarse sand	1.87	1.18	0.30	0.65
U1396A-4H-7, 73–75	Bimodal	Poorly sorted coarse sand	1.21	1.41	0.38	1.10
U1396A-5H-1, 19–21	Trimodal	Poorly sorted medium sand	1.79	1.24	0.07	0.81
U1396A-5H-1, 30–32	Bimodal	Poorly sorted coarse sand	1.32	1.46	0.34	0.71

Table T3 (continued).

Hole, core, section, interval (cm)	Distribution type	Sediment name	Mean (M_Z)	Sorting (σ_I)	Skewness (Sk_I)	Kurtosis (K_G)
U1396A-5H-1, 35–37	Bimodal	Moderately sorted very fine sand	2.84	0.87	–0.41	0.84
U1396A-5H-1, 43–45	Bimodal	Poorly sorted coarse sand	0.49	1.02	0.28	1.39
U1396A-5H-1, 46–47	Bimodal	Moderately sorted coarse sand	0.89	0.82	0.22	1.32
U1396A-5H-1, 53–54	Bimodal	Moderately sorted coarse sand	0.97	0.95	0.32	1.36
U1396A-5H-1, 59–61	Unimodal	Moderately sorted coarse sand	0.82	0.90	0.25	1.37
U1396A-5H-1, 65–66	Trimodal	Poorly sorted fine sand	2.29	1.02	–0.12	0.78
U1396A-5H-1, 68–69	Bimodal	Poorly sorted coarse sand	1.24	1.48	0.35	0.76
U1396A-5H-2, 76–77	Unimodal	Moderately sorted very fine sand	2.80	0.73	–0.11	0.75
U1396A-5H-5, 32–33	Bimodal	Moderately sorted medium sand	1.39	0.88	0.34	1.30
U1396A-5H-6, 44–45	Unimodal	Moderately well sorted very fine sand	3.01	0.56	–0.11	0.86
U1396A-6H-4, 18–19	Unimodal	Moderately well sorted very fine sand	2.95	0.67	–0.21	0.91
U1396A-6H-4, 47–48	Trimodal	Moderately sorted medium sand	2.22	0.99	0.25	0.71
U1396A-6H-4, 61–62	Bimodal	Moderately sorted medium sand	2.03	0.80	0.15	1.02
U1396A-6H-4, 70–71	Bimodal	Moderately sorted medium sand	2.03	0.78	0.11	0.97
U1396A-6H-4, 77–78	Unimodal	Moderately sorted very coarse sand	-0.12	0.76	0.34	2.07
U1396A-6H-4, 80–82	Unimodal	Moderately sorted very coarse sand	-0.03	0.77	0.30	1.81
U1396A-6H-4, 82–83	Unimodal	Moderately well sorted medium sand	1.13	0.69	–0.02	0.96
U1396A-6H-4, 84–85	Unimodal	Moderately well sorted coarse sand	0.90	0.52	0.01	0.95
U1396A-6H-4, 87–88	Unimodal	Moderately well sorted coarse sand	0.56	0.52	–0.01	0.94
U1396A-6H-4, 90–92	Unimodal	Moderately well sorted medium sand	1.16	0.55	0.17	1.06
U1396A-6H-4, 94–95	Unimodal	Moderately well sorted fine sand	2.20	0.52	0.02	0.94
U1396A-6H-5, 50–51	Bimodal	Moderately sorted coarse sand	0.97	0.88	0.16	1.15
U1396A-6H-5, 54–55	Bimodal	Poorly sorted coarse sand	0.77	1.17	0.30	1.14
U1396A-6H-5, 58–59	Unimodal	Moderately well sorted coarse sand	0.45	0.66	0.03	0.98
U1396A-6H-5, 144–145	Unimodal	Moderately sorted very fine sand	2.88	0.74	–0.23	0.92
U1396A-6H-6, 3–4	Unimodal	Very well sorted very fine sand	3.47	0.30	–0.25	0.84
U1396A-6H-6, 121–122	Unimodal	Moderately well sorted fine sand	2.77	0.70	–0.07	0.84
U1396A-6H-6, 146–147	Unimodal	Well sorted very fine sand	3.31	0.43	–0.28	0.87
U1396A-6H-7, 5–6	Unimodal	Moderately well sorted very fine sand	2.97	0.67	–0.25	0.88
U1396A-6H-7, 35–36	Polymodal	Poorly sorted fine sand	2.26	1.01	–0.04	0.79
U1396A-6H-7, 39–40	Bimodal	Moderately sorted medium sand	1.59	0.92	0.12	1.02

Table T4. Summary statistics on the grain size data presented in Table T3.

Mean	Count	Sorting	Count	Skewness	Count	Kurtosis	Count	Distribution	Count
Very fine sand	3	Poorly sorted	21	Very fine skewed	12	Very platykurtic	3	Unimodal	30
Fine sand	23	Moderately sorted	28	Fine skewed	18	Platykurtic	23	Bimodal	29
Medium sand	25	Moderately well sorted	18	Symmetrical	26	Mesokurtic	30	Trimodal	8
Coarse sand	16	Well sorted	1	Coarse skewed	11	Leptokurtic	11	Polymodal	2
Very coarse sand	2	Very well sorted	1	Very coarse skewed	2	Very leptokurtic	2		